Energy Advances

ROYAL SOCIETY OF CHEMISTRY

PAPER

View Article Online
View Journal | View Issue

Cite this: *Energy Adv.*, 2026, 5, 528

Enhanced Cr(VI) removal and power generation in tannery wastewater using ORR-optimized cathodes in single-chamber microbial fuel cells

Dena Z. Khater,[a] R. S. Amin,[a] Amani E. Fetohi,[a] Mohamed Mahmoud[b] and K. M. El-Khatib *[a]

The environment and human health are seriously threatened by hazardous heavy metals, including hexavalent chromium [Cr(VI)], due to its toxicity and mobility. Single-chamber microbial fuel cells (MFCs) offer a simple, cost-effective configuration and an emerging technology for bioremediation of Cr(VI)-containing tannery wastewater into renewable energy. This study proposes a straightforward strategy to enhance Cr(VI) bioremediation and electricity generation in MFCs treating real tannery wastewater. This approach involves optimizing the anodic biofilm to sustain organic degradation under high Cr(VI) concentrations and developing low-cost, highly active oxygen reduction reaction (ORR) cathodes to replace precious metal catalysts such as Pt/C. In the optimized configuration, the MFCs achieved a Cr(VI) removal efficiency of 93.05 ± 2.35, 90.14 ± 5.8, 85.83 ± 4.8, and 73.61 ± 5.53% with a Coulombic efficiency of 37.09 ± 4.85, 31.04 ± 3.08, 26.74 ± 3.16, and 21.1 ± 23.29% for Pt/C, Ag_2O–MnO_2/rGO–NiPc, PdO–MnO_2/rGO, and control MFC, demonstrating the system's strong environmental performance. Additionally, tannery MFCs (TMFCs) equipped with Pt/C and Ag_2O–MnO_2/rGO–NiPc cathodes exhibited relatively higher power output (*i.e.*, 24.76 and 21.14 mW m^{-3}, respectively) compared with PdO–MnO_2/rGO–TMFC (19.94 mW m^{-3}) and the control TMFC (13.21 mW m^{-3}). These findings offer a promising strategy for effective chromium remediation in treating tannery wastewater streams.

Received 14th October 2025,
Accepted 23rd February 2026

DOI: 10.1039/d5ya00299k

rsc.li/energy-advances

1. Introduction

Pollution due to heavy metals (*e.g.*, cadmium (Cd), mercury (Hg), lead (Pb), arsenic (As), and chromium (Cr)) remains one of the major environmental challenges facing our society, owing to their non-biodegradable nature and toxicity, resulting in a significant adverse impact on human health and ecological well-being.[1] In this context, chromium pollution, particularly due to hexavalent chromium (Cr(VI)), which has been recognized as one of the most carcinogenic toxins, poses devastating risks to human health due to its high solubility, toxicity, and mobility in the environment.[2] Hexavalent chromium is widely utilized in various industrial applications, including leather tanning, whose waste streams are characterized by a high level of Cr(VI).[3,4] Due to the significant health risks posed by Cr(VI) exposure, the United States Environmental Protection Agency (US EPA) has set permissible limits for this contaminant in drinking water (0.05 ppm) and wastewater discharge (0.1–0.5 ppm).[5] The ideal remediation approach for addressing Cr(VI)-contaminated effluents involves reducing the hazardous Cr(VI) to the less harmful Cr(III). Various traditional technologies have been used for the reduction of Cr(VI) to Cr(III), including adsorption, ion exchange, and membrane filtration; however, these technologies tend to be energy-consuming, and the handling of the resultant sludge incurs high costs.[6,7]

Among potential Cr(VI) remediation technologies, bioremediation, which relies on the metabolic capabilities of microbes to convert a wide range of inorganic contaminants into non-harmful byproducts, can address certain limitations of physical–chemical technologies while also being an energy-efficient and cost-effective solution.[8,9] Microbes inherently employ various strategies to endure in chromium-contaminated environments through the integration of different mechanisms, including biosorption, bioaccumulation, and biotransformation, which facilitate the biological reduction of toxic Cr(VI) into Cr(III).[10] However, the performance of these technologies is often constrained by several operational challenges, such as high energy demand, significant chemical consumption, and substantial capital investment. Additionally, many of these processes generate large volumes of concentrated sludge,

[a] *Chemical Engineering & Pilot Plant Department, Engineering Research and Renewable Energy Institute, National Research Centre, 33 El-Buhouth St., Dokki, Cairo 12622, Egypt. E-mail: kamelced@hotmail.com*
[b] *Water Pollution Research Department, National Research Centre, 33 El-Buhouth St., Dokki, Cairo 12622, Egypt*

further complicating disposal and environmental compliance. Given these limitations, the development of cost-effective and sustainable alternatives for treating Cr(VI)-contaminated tannery wastewater is urgently needed.[11] In this context, microbial electrochemical systems, including microbial fuel cells (MFCs), have been employed as a sustainable approach for the remediation of various contaminants while simultaneously generating renewable energy.[12–15] In a typical MFC, a diverse microbial consortium facilitates the oxidation or reduction of a specific contaminant by using external solid electrodes as limitless electron acceptors or donors.[16–19] Recent studies have shown that microbial fuel cells (MFCs) exhibit high efficiency in the cathodic reduction of Cr(VI) coupled with low-grade organic matter in the anode chamber, producing renewable electricity.[20,21] For example, Khater *et al.*[22] demonstrated effective Cr(VI) reduction in the cathode of dual-chamber MFCs fed with a wide range of initial Cr(VI) concentrations (5–60 ppm), with high power density production (195.1 mW m^{-3}). Microbial community analysis revealed that this high Cr(VI) reduction efficiency is likely due to the development of a robust, diverse biocathode that catalyzes the bioreduction of Cr(VI) to less harmful Cr(III), as evidenced by X-ray photoelectron spectroscopy (XPS) analysis. In another study, Li *et al.*[23] showed almost complete abiotic reduction of Cr(VI) in a double-chamber MFC fed with real electroplating wastewater, even with a high Cr(VI) concentration of 204 ppm. This high efficiency of MFC in reducing Cr(VI) was accompanied by a maximum power density of 1.6 W m^{-2} at a Coulombic efficiency (CE) of 12%. However, using MFCs for remediating Cr(VI)-contaminated water bodies remains challenging owing to limited cathodic mass transfer, necessitating improvements in cathode characteristics to expedite Cr(VI) reduction.[24]

To tackle this technical challenge, there has been a growing interest in developing cost-effective, advanced materials to improve the cathode's electrochemical catalytic activity and electrical conductivity, thereby enhancing the overall performance of MFCs, in terms of boosting electricity generation and pollutant biodegradation.[25–28] Recent studies have demonstrated that decorating the cathode surface with highly efficient oxygen reduction reaction (ORR) catalysts significantly enhances the Cr(VI) reduction efficiency in microbial fuel cells (MFCs) compared to control MFCs equipped with pristine carbon-based cathodes, likely due to a decrease in cathode activation overpotential and an increase in exposed surface area.[29,30] For instance, Fei *et al.*[31] employed an MFC equipped with a reticulated vitreous carbon (RVC) cathode modified with carbon nanotubes (CNT) for Cr(VI) removal and electricity generation. The MFC equipped with the RVC–CNT cathode exhibited a much higher power density of 132.1 mW m^{-2} and Cr(VI) removal of 80.9%, compared to 55.0 mW m^{-2} and 44.5% for a control MFC with an unmodified RVC cathode. In a more recent study, Ali *et al.*[32] observed a complete Cr(VI) removal in a dual-chamber MFC-equipped FeS@-rGO cathode, which was nearly 4.6-fold higher than a control MFC. This high efficiency for Cr(VI) removal was accompanied by generating a much higher maximum power density of 154 mW m^{-2} compared to only 36 mW m^{-2} for the control MFC.

Building on our previous findings, we hypothesized that PdO and MnO_2 nanoparticles embedded within a reduced graphene oxide (rGO) framework (PdO–MO_x/rGO) and Ag_2O and MnO_2 nanoparticles supported on reduced graphene oxide (rGO) and nickel phthalocyanine (NiPc) framework (Ag_2O–MnO_2/rGO–NiPc) cathodic electrocatalysts can alter the cathodic surface in single-chamber MFCs for enhancing Cr(VI) reduction and electricity generation.

The specific objectives of this study were to:

- Evaluate the performance of MFCs operated with a wide range of influent Cr(VI) concentrations (5–60 mg L^{-1}), focusing on electricity generation, Cr(VI) reduction efficiency, and determination of the maximum tolerable concentration (MTC).
- Enhance cathodic performance by modifying the cathode surface with thin layers of PdO–MnO_2/rGO and Ag_2O–MnO_2/rGO–NiPc electrocatalysts, and compare the long-term efficiency of these modified cathodes against a control MFC equipped with plain carbon cloth.
- Investigate the role and mechanisms of the modified cathodes in promoting Cr(VI) bioreduction during treatment of real tannery wastewater, including analysis of electrochemical behavior and bioremediation pathways.

Collectively, these objectives aim to demonstrate the potential of microbial fuel cells as an effective, sustainable technology for removing toxic Cr(VI) from tannery wastewater while generating renewable energy.

2. Materials and methods

2.1. Preparation of electrocatalysts and cathode electrodes

We synthesized PdO–MnO_2/rGO and Ag_2O–MnO_2/rGO–NiPc electrocatalysts using the surfactant-mediated templating technique as described in our previous studies, respectively[33,34] rGO was prepared using a modified Hummers' method. Briefly, graphite was oxidized in a H_2SO_4/H_3PO_4 mixture with $KMnO_4$ under controlled temperature, followed by dilution, peroxide treatment, and acid washing to remove metal residues. The resulting GO was repeatedly rinsed to pH = 5.5 and dried at 80 °C. Both PdO–MnO_2/rGO and Ag_2O–MnO_2/rGO–NiPc electrocatalysts were produced *via* a surfactant-mediated templating method using cetyltrimethylammonium bromide (CTAB) to control particle dispersion and morphology. The resulting composites contained approximately 30 wt% total metal oxides (PdO–MnO_2 or Ag_2O–MnO_2) and 70 wt% rGO-based material. For PdO–MnO_2/rGO, 250 mg CTAB was dissolved in ethylene glycol (50 mL) and ultrasonicated for 0.5 h. Metal nitrate precursors (160 mg) and $Pd(NO_3)_2$ (0.15 g) were added under vigorous stirring for 2 h while maintaining a pH of 10 with 1 M NaOH. GO (0.4 g) was then incorporated, followed by an additional 0.5 h of stirring and ultrasonication. The mixture was transferred to a Teflon-lined autoclave and heated at 160 °C for 4 h. The product was washed, dried at 80 °C for 6 h, and calcined at 500 °C for 4 h. For Ag_2O–MnO_2/rGO–NiPc, NiPc and GO were first mixed in H_2SO_4 (40 mL) at a NiPc : GO ratio of 1 : 3%, stirred for 3 h in an ice bath, washed to pH = 5, and dried

to form the GO–NiPc intermediate. The subsequent hydrothermal synthesis followed the same procedure as described for PdO–MnO_2/rGO.

Afterwards, we modified the gas-diffusion carbon cloth electrodes (a projected surface area of 16.63 cm^2; Fuel Cell Store, TX, USA) by depositing a thin layer of the as-prepared electrocatalysts. To prepare the electrocatalyst layer, we mixed the electrocatalysts with 0.5 mL of Nafion solution (5%; Sigma-Aldrich, USA) and ultrasonicated the mixture for 30 minutes at 60 °C. After obtaining uniform electrocatalyst inks, we deposited successive layers of the inks on the cathode surface, achieving the desired mass loading of ~0.3 mg cm^{-2}. We also prepared a control cathode with a benchmark Pt/C catalyst at a mass loading of ~0.3 mg cm^{-2}, following the same procedure as described previously. Finally, all electrodes were dried at room temperature overnight before being used in the MFC experiments, and no additional thermal treatment was performed beyond drying.

2.2. MFC setup and operation

Single-chamber MFCs were constructed from plexiglass with a working volume of 100 mL. The anodes were 3-dimensional carbon felt (Fuel Cell Store, TX, USA) with a projected anodic surface area of 18.50 cm^2. The cathodes were made of gas-diffusion carbon cloth electrodes coated with the prepared thin layer of electrocatalyst, as previously described. Titanium wires were used as current collectors to connect the anode and cathode electrodes. Before starting the MFCs' operation, all bioreactors were inoculated with anaerobic sludge from a local sewage treatment facility (Benha, Egypt). All MFCs were operated in a fed-batch mode and supplemented with an artificial growth medium containing: glucose: 1 g L^{-1}; $NaHCO_3$: 2.5 g L^{-1}; NH_4Cl: 0.2 g L^{-1}; H_2PO_4: 13.6 g L^{-1}; KCl: 0.33 g L^{-1}; NaCl: 0.3 g L^{-1}; K_2HPO_4: 17.4 g L^{-1}; $CaCl_2{\cdot}2H_2O$: 0.15 g L^{-1}; $MgCl_2$: 3.15 g L^{-1}; yeast extract: 1 g L^{-1}; and 12.5 mL of trace metal solution. All experiments were carried out at room temperature (25 ± 2 °C), with the MFC cathode operated under passive aeration, and oxygen supplied solely by natural diffusion through the cathode layer; no external airflow or forced aeration was applied, and the MFC operated in batch-fed mode for an adaptation period of 75 days.

Following the acclimation period, we studied the impact of Cr(VI) on the steady-state performance of MFCs by stepwise increasing the influent Cr(VI) concentration from 5 to 60 mg L^{-1}. After estimating the maximum tolerable concentration of Cr(VI), MFCs were operated and fed with a 50 mM phosphate buffer solution containing 30 mg L^{-1} of Cr(VI). Finally, we fed MFCs with real tannery wastewater (TMFCs) collected from a local factory in Giza, Egypt, for leather and tanning products. Upon collection, we immediately transported the tannery wastewater to our laboratory and stored it at 4 °C before use. Table 1 showed the main characteristics of tannery wastewater used in this study. As noted, this wastewater has a high pH (12.8), elevated salinity, and a high organic load, which pose practical operational challenges but more accurately reflect actual treatment needs.

During our study, raw tannery wastewater was used as received without dilution, pH correction, or macronutrient addition to assess MFC performance under realistic industrial conditions. For comparison, we operated two sets of control bioreactors: the first was a single-chamber MFC equipped with a Pt/C cathode, and the other was a single-chamber MFC with a plain carbon cloth cathode (no catalyst layer). All experiments were conducted at room temperature (25 ± 2 °C) in triplicate to verify reproducibility and feasibility of operation.

2.3. MFC analysis and calculation

The potential output of MFCs under an external resistance of 10 kΩ was measured using a data acquisition system (LabJack U6-PRO, USA) at 5 min intervals. In addition, polarization curves were obtained by varying the external resistance (R_{ext}) from 500 Ω to 1 MΩ using an R-BOX 01-decade resistor box. We operated MFCs for 30 minutes at each R_{ext} to achieve pseudo-stable-state operation. The internal resistances (R_{in}) were estimated from the slope of the linear region of the polarization curves. Volumetric current density (j, mA m^{-3}) and power density (PD, mW m^{-3}) were estimated using Ohm's law, and normalized to the overall MFC volume (*i.e.*, 100 mL). Chemical oxygen demand (COD) was measured according to the method described in the Standard Methods for the examination of Water and Wastewater.[35] The Coulombic efficiency (CE) was calculated by dividing the recovered electron

Table 1 Physicochemical characteristics of tannery wastewater used in this study (average ± standard deviation)

Tannery wastewater parameters	Unit	Pre-treatment	Post-treatment
pH	—	12.8 ± 0.51	7.8 ± 0.71
Total chromium	mg L^{-1}	3.6 ± 0.53	0.57 ± 0.19
Total dissolved solids (TDS)	mg L^{-1}	15023 ± 238	12570 ± 153
Electrical conductivity	mS cm^{-1}	20.2 ± 1.2	12.3 ± 1.2
Chemical oxygen demand (COD)	mg L^{-1}	7298 ± 616	1452 ± 54
Biochemical oxygen demand (5-day) (BOD_5)	mg L^{-1}	3103 ± 343	256 ± 6
Total suspended solids	mg L^{-1}	3122 ± 460	1156 ± 56
Total nitrogen (TN)	mg L^{-1}	820 ± 160	115 ± 72
Ammonia	mg L^{-1}	310 ± 130	98 ± 54
Nitrate	mg L^{-1}	340 ± 98	102 ± 56
Phosphate (PO_4^-)	mg L^{-1}	25 ± 3.4	8 ± 1.2
Sulfate (SO_4^{2-})	mg L^{-1}	2400 ± 230	568 ± 4.1
Color	—	Dark brown	Light brown

equivalents at the anode, measured as current density, by the total organic matter consumed by the electroactive biofilm.[36]

$$\mathrm{CE} = \frac{\mathrm{CP}}{\mathrm{CT}} \times 100 = \frac{MIt}{FbV\Delta\mathrm{COD}} \quad (1)$$

where M is the molecular weight of oxygen (32 g mol^{-1}), I is the current (A), t is the operation time for closed circuit (s), F is Faraday's constant (96 485 C mol^{-1}), b is the number of electrons exchanged per mole of oxygen (4), ΔCOD is the difference in COD before and after treatment (g L^{-1}), and V is the volume of the electrolyte (L).

Chromium specification in the influent was determined by measuring total Cr concentrations after acidic pre-treatment using inductively coupled plasma (ICP-OES; Agilent ICP-OES 5100, Australia) to confirm the Cr fraction present in the raw wastewater. The removal efficiency (Cr R%) was estimated as follows:

$$\mathrm{Cr}\ R\% = \frac{\mathrm{Cr_{inf}} - \mathrm{Cr_{eff}}}{\mathrm{Cr_{inf}}} \times 100 \quad (2)$$

where $\mathrm{Cr_{inf}}$ and $\mathrm{Cr_{eff}}$ are the Cr(VI) concentrations in the influent and effluent of MFCs.

At the end of the batch operation, the MFC electrodes were collected to study the change in their surface after exposure to high Cr(VI) concentrations using X-ray photoelectron spectroscopy (XPS) as described elsewhere.[22]

3. Results and discussion

3.1. Efficiency of MFC fed with different Cr(VI) concentrations

We developed an electroactive anodic biofilm by feeding MFCs with a PBS growth medium containing glucose as the sole donor substrate for 75 days (Fig. 1a). Our results showed a gradual increase in the open-circuit potential (OCP) until reaching its maximum value (*i.e.*, 0.45 ± 0.01 V) after 45 days, implying the successful formation of a robust anodic biofilm, which was capable of efficiently oxidizing organic matter and respiring the resulting electrons into the anode surface.[37,38]

Following the successful formation of an electroactive anodic biofilm, we fed control MFCs equipped with plain carbon cathodes with growth media containing different Cr(VI) concentrations (*i.e.*, 5–60 mg L^{-1}). Fig. 1b shows that both the maximum closed-circuit potential and the volumetric PD increased with increasing initial Cr(VI) concentration from 5 to 30 mg L^{-1}. However, a further increase in the initial Cr(VI) concentration resulted in a sharp decrease in potential output and volumetric PD, suggesting acute inhibition of the electroactive biofilm. Our results were in agreement with previous studies, showing that any Cr(VI) higher than the MTC can inhibit the growth of an electroactive biofilm and cause irreversible damage to microbial DNA, resulting in the production of low potential output.[22,29,39] Furthermore, we observed that the Cr(VI) removal efficiency gradually increased as the initial Cr(VI) concentrations increased, achieving its peak (84 ± 3%) at an initial Cr(VI) concentration of 30 mg L^{-1}. However, when the initial Cr(VI) concentrations exceeded the MTC, the Cr(VI) removal efficiency decreased significantly (Fig. 1c). We also observed that the conversion of the donor substrate into electricity (expressed as CE) was affected by the initial Cr(VI) concentrations, with the highest CE achieved at an initial Cr(VI) concentration of 30 mg L^{-1}.

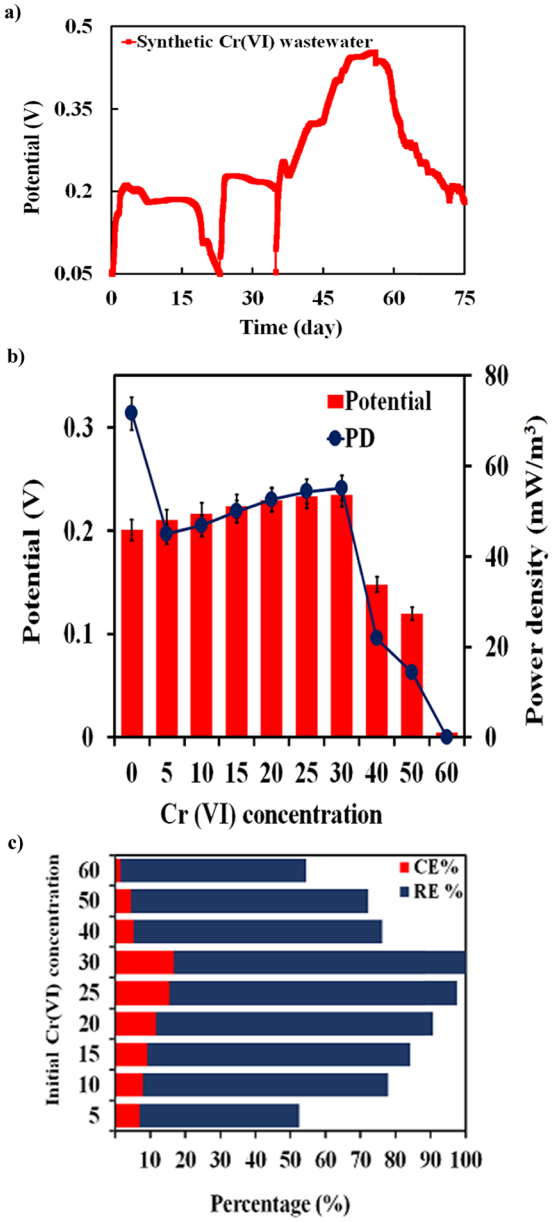

Fig. 1 Performance of control MFCs equipped with plain carbon cloth cathodes: (a) open-circuit potential output during the acclimation phase, (b) maximum closed-circuit potential and volumetric power density of MFCs fed with different initial Cr(VI) concentrations (error bars indicate the relative standard deviation of two replicates), and (c) Coulombic efficiency (CE) and Cr(VI) removal efficiencies (REs).

This trend reflects a trade-off between increased electron-acceptor availability and biomass toxicity. At moderate Cr(VI) concentrations (up to 30 mg L^{-1}), the added chromate serves as an efficient terminal electron acceptor, stimulating microbial respiration and enhancing electron transfer to the anode,

thereby improving Cr(VI) reduction. However, beyond this threshold, Cr(VI) becomes increasingly toxic to the electroactive biofilm: its strong oxidizing character causes oxidative stress, membrane damage, and enzyme inhibition, which suppress metabolic activity, slow donor substrate oxidation, and ultimately reduce the electron flux available for Cr(VI) reduction. This toxicity-driven decline in biofilm performance outweighs the benefit of increased Cr(VI) concentration, resulting in the observed decrease in removal efficiency at higher concentrations. Collectively, our findings indicate that the overall performance of MFCs was mainly linked to the toxicity of Cr(VI) on anodic microbes, as well as cathode activation overpotential and exposed surface area.

Previous studies showed that Cr(VI) induces toxicity primarily through the generation of intracellular reactive oxygen species, disruption of membrane integrity, and interference with essential metabolic and respiratory enzymes.[40] In electroactive consortia, dissimilatory metal-reducing bacteria (DMRB) such as *Geobacter* spp. and *Shewanella* spp. are particularly sensitive to oxidative damage because Cr(VI) and its reactive intermediates impair outer-membrane cytochromes and periplasmic redox proteins crucial for extracellular electron transfer (EET).[41]

Moreover, Cr(VI) can interact with functional groups in extracellular polymeric substances (EPS), including C–O, C═O, and aromatic/quinone moieties, resulting in structural modification of the biofilm matrix and reduced efficiency of electron shuttling.[42] These combined effects suggest that elevated Cr(VI) levels can selectively inhibit highly electroactive microbial populations and destabilize functional groups essential for extracellular electron transfer (EET), consistent with the changes in biofilm composition and XPS surface chemistry observed in this study. Despite these inhibitory mechanisms, the biofilm retained measurable Cr(VI) reduction activity, indicating the presence of chromium-resistant microbes and protective EPS components that mitigate toxicity.[43]

We employed XPS analysis to examine changes in the anode's surface chemistry after exposure to a high level of Cr(VI) (*i.e.*, 30 mg L^{-1}). As illustrated in Fig. 2a, the wide-spectrum survey showed six major peaks at binding energies of 291.58, 540.58, 300.08, 143.08, 206.58, and 598.62 eV, which were associated with C 1s, O 1s, K 2p, P 2p, Cl 2p, and Cr 2p, respectively.[44] Furthermore, it could be noticed that the C 1s spectra were fitted to the three main characteristic peaks at binding energies of 284.92 (C–C/C═C), 286.08 (C–O), and 288.62 (C═O) eV.[45] In addition, the O1 spectra were deconvoluted into three single peaks with binding energies of 531.2, 532.11, and 532.47 eV corresponding to C═O, C–OH, and O–(C═O)–C, respectively.[46] The Cr 2p spectra showed that there were four distinct peaks at binding energies of 577.23 and 580.08 eV (Cr $2p_{3/2}$) that were correlated with the presence of Cr(III) and 584.6 and 588.18 eV (Cr $2p_{1/2}$) that were assigned to Cr(VI). This pattern suggests that bioabsorption of Cr(III) probably occurred through interactions with C–H, C–C, C═O, C–OH, and O–C═O functional groups present in bacterial cells, which primarily exist as $Cr(OH)_3$ and Cr_2O_3.[47,48] As shown in Fig. 2b, the proposed mechanism in the SCMFC involves the direct bioreduction of toxic, mobile Cr(VI) by acclimated dissimilatory metal-reducing bacteria (DMRB), including *Geobacter* spp., *Shewanella* spp., *Pseudomonas* spp., *Bacillus* spp., and *Desulfovibrio* spp., on the anode surface. During this process, Cr(VI) binds to functional groups (*e.g.*, C–O, C═O) on the DMRB

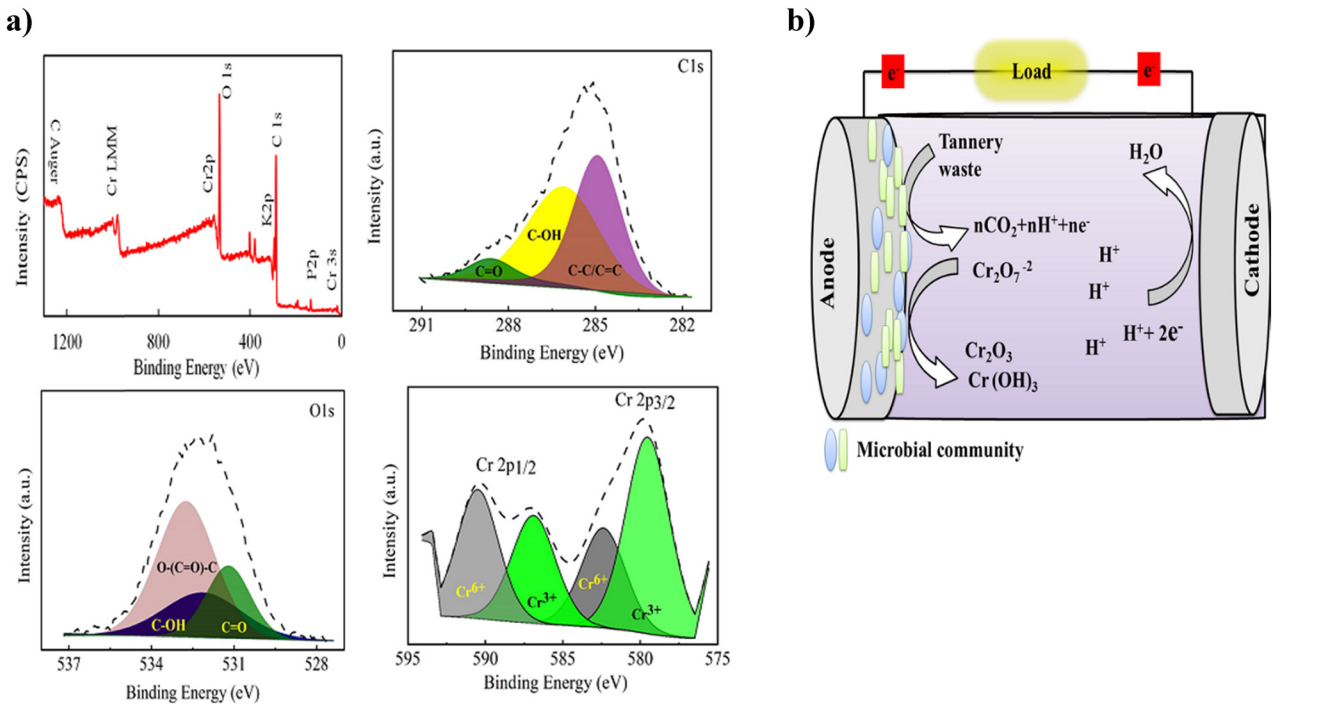

Fig. 2 (a) XPS analysis of anode electrodes after exposure to a high level of Cr(VI) and (b) the proposed Cr(VI) removal mechanism.

cell surface, facilitating chemical interactions that position Cr(VI) for enzymatic reduction. Chromate reductase then catalyzes the reduction of Cr(VI) to the less toxic and less mobile Cr(III) form, which subsequently becomes immobilized within the biofilm, primarily as $Cr(OH)_3$ and Cr_2O_3. This pathway effectively minimizes environmental impact by preventing the release of soluble chromium species.

3.2. Performance of MFCs equipped with different cathodic electrocatalysts at MTC

Following the successful development of robust microbial consortia, we constructed MFCs equipped with different cathodic electrocatalysts to test whether cathode materials can improve the bioreduction efficiency of Cr(VI). All MFCs were operated in batch-fed mode with a growth medium containing a constant Cr(VI) concentration of 30 mg L^{-1} for 30 days under open-circuit conditions. This mode allows the microbial communities to acclimate to high levels of Cr(VI) in the influent.[39] During the adaptation period, we observed that the MFC equipped with Ag_2O–MnO_2/rGO–NiPc cathode (Ag_2O–MnO_2/rGO–NiPc–MFC) exhibited a superior activity, as evidenced by higher open-circuit potential (OCP) (*i.e.*, 0.62 ± 0.11 V) compared to PdO–MnO_2/rGO–MFC (0.56 ± 0.10 V), and control MFC (0.46 ± 0.09 V). Then, MFCs were operated under closed-circuit mode with a fixed resistance of 10 kΩ (Fig. 3a). Consistent with OCP data, Ag_2O–MnO_2/rGO–NiPc–MFC showed the highest maximum closed-circuit potential of 0.47 ± 0.08 V, which was 1.34–1.95-fold higher than that of PdO–MnO_2/rGO–MFC and control MFC.

We also evaluated the efficiency of MFCs equipped with different cathodes by constructing polarization and power output curves. We gradually varied the external resistances between 1 MΩ and 500 Ω and measured the potential output. We observed that the Ag_2O–MnO_2/rGO–NiPc-MFC produced the highest maximum PD (PD_{max}) of 241.4 mW m^{-3} (91.35 mW m^{-2}) at volumetric j of 92.9 mA m^{-3} value which was 1.44–3.11-fold higher than that of PdO–MnO_2/rGO-MFC at PD of 167.2 mW m^{-3} (63.27 mW m^{-2}) and control MFC at PD of 77.6 mW m^{-3} (29.35 mW m^{-2}) (Fig. 3b). The internal resistance (R_{in}) of MFCs was estimated by conducting linear regression of the Ohmic region of the polarization curves (Fig. 3c). Among all MFCs, Ag_2O–MnO_2/rGO–NiPc–MFC had the lowest R_{in} of 127 ± 1.5 Ω, which was significantly lower than that of PdO–MnO_2/rGO–MFC (211 ± 4.1 Ω) and control MFC (284 ± 4.8 Ω). Since we used similar experimental conditions for MFCs (*e.g.*, MFC design, substrate type, anode material, and working volume), the variation in MFC internal resistance can be ascribed solely to the electrocatalytic characteristics of the cathodic electrocatalysts. Thus, our results demonstrated that the Ag_2O–MnO_2/rGO–NiPc catalyst serves as an ideal cathode material for improving the electrochemical characteristics of carbon cloth cathodes, thereby favoring Cr(VI) reduction and electricity generation in MFCs.[49]

The Cr(VI) removal efficiency in MFCs showed a similar trend to power generation, with Ag_2O–MnO_2/rGO–NiPc–MFC exhibiting the highest removal efficiency of 90.78 ± 0.65% compared to 88.01 ± 1.37% for PdO–MnO_2/rGO–MFC and 83.15 ± 1.4%

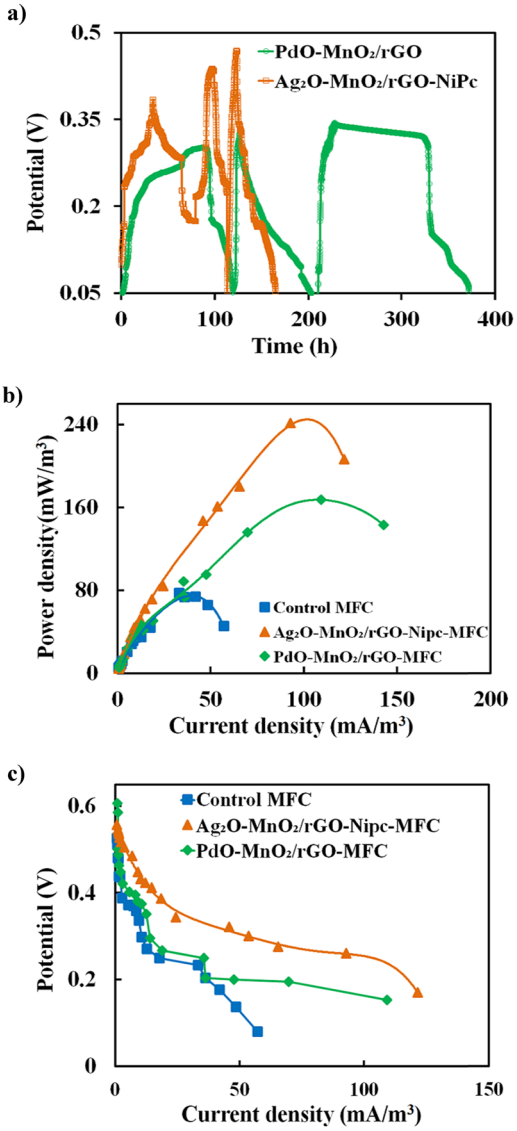

Fig. 3 Performance of MFCs equipped with different cathodes and fed with 30 mg Cr(VI)/L-containing growth media: (a) closed-circuit potential output, (b) power curve, and (c) polarization curve.

for control MFCs. Furthermore, the Ag_2O–MnO_2/rGO–NiPc–MFC showed the highest coulombic efficiency (CE) of 25.38 ± 0.15% compared to 19.23 ± 0.84% for PdO–MnO_2/rGO-MFC and 16.11 ± 86% for the control MFC. The Cr(VI) reduction at the cathode in single-chamber MFCs occurs through a set of interconnected pathways. Chromate (CrO_4^{2-}) or dichromate ($Cr_2O_7^{2-}$) can undergo direct electrochemical reduction at the cathode surface when delivered from the anode. In this pathway, electrons reduce Cr(VI) through intermediate valence states (*e.g.*, Cr(V), Cr(IV)) to form Cr(III), which subsequently precipitates as $Cr(OH)_3$ or forms Cr_2O_3. This reaction was strongly influenced by the cathode material's catalytic activity, conductivity, and surface chemistry. Catalysts with higher electron-transfer rates (*e.g.*, Pt/C or ORR-optimized nanocomposites) deliver electrons to Cr(VI) more efficiently, thereby accelerating

its reduction. The contribution of ORR activity in driving Cr(VI) reduction enhances reduction indirectly by improving the cathode's overall redox environment. ORR-active catalysts raise the cathode potential and lower the cathodic overpotentials, thereby improving the driving force for electron flow from the anode to the cathode. This results in higher electron flux and lower charge-transfer resistance. Thus, ORR activity does not simply compete with Cr(VI) reduction; rather, it strengthens the entire cathodic electron-transfer framework, indirectly benefiting Cr(VI) removal. Although most microbial activity occurs at the anode, microbial processes indirectly support cathodic Cr(VI) reduction by releasing electrons and maintaining an anodic biofilm.

In addition, highly active ORR catalysts significantly influence overall MFC performance by reducing internal resistance, especially the charge-transfer component. A cathode with superior ORR kinetics enhances electron acceptance, lowers circuit resistance, boosts power density, and improves Cr(VI) reduction. Therefore, ORR catalytic performance was directly tied to both energy recovery and pollutant removal efficiency.[50] Cathodes with high ORR activity not only generate more power but also enable more rapid and complete Cr(VI) reduction due to improved electron transfer dynamics.[51,52]

Thus, modification of the cathodic surface with mixed metal oxides reduces internal resistance, enhances electron transfer, and facilitates electrostatic interactions with Cr(VI), thereby improving the efficiency of MFCs for bioenergy generation and Cr(VI) reduction. Therefore, SCMFCs have great potential for the detoxification of Cr(VI) contamination sites due to their low operating costs, self-regeneration, and sustainable power supply.[53] Our results signify the crucial role of cathodic electrocatalysts in enhancing electricity generation in MFCs fed with toxic substrates (*e.g.*, Cr(VI)-containing waste streams).[53]

3.3. Evaluation and treatment of tannery wastewater in MFCs

The physicochemical characteristics of tannery wastewater were assessed pre and post-bacterial treatment, and the results were summarized in Table 1. The data clearly indicated that the untreated effluent contains exceptionally high levels of hazardous substances, making it a major source of environmental pollution. The key measured parameters for the raw effluent included: pH (12.8 ± 0.5), TDS (15 023 ± 238 mg L^{-1}), BOD_5 (3103 ± 343 mg L^{-1}), COD (7298 ± 616 mg L^{-1}), sulfate (SO_4^{2-}) (2400 ± 230 mg L^{-1}), and total chromium (3.6 ± 0.53 mg L^{-1}). The final pollutant levels were evaluated against typical tannery discharge limits at the order-of-magnitude scale. The post-treatment Cr(VI) concentration (0.57 ± 0.19 mg L^{-1}) falls within internationally reported chromium discharge ranges (0.05–10 mg L^{-1} for direct discharge; 1–50 mg L^{-1} for sewer systems), indicating effective Cr(VI) reduction. In contrast, the final COD value (1452 ± 54 mg L^{-1}) remains higher than levels typically required for compliant discharge, which were generally in the low hundred's mg L^{-1} after advanced treatment, despite being lower than the high-strength raw wastewater commonly reported at 2000–15 000 mg L^{-1}. This suggests that further treatment would be necessary to meet stringent COD standards. Following bacterial treatment in SCMFCs, these values showed substantial reductions. This decline can be attributed to the biodegradation of inorganic and complex organic pollutants facilitated by the active DMRB community on the anodic surface. The removal mechanisms likely involved metal bioaccumulation within microbial cells and/or biosorption onto the bacterial cell surface.

We also assessed the efficacy of MFCs with an acclimated anodic biofilm and different cathodes for the treatment of high-strength tannery wastewater, while concurrently generating renewable electricity. The high-strength wastewater stream was characterized by a high organic matter content (*i.e.*, 7298 ± 616 mg COD per L), a relatively high biodegradability ratio of 0.43 ± 0.06%, and a moderate Cr concentration of 3.6 ± 0.53 mg L^{-1}. We fed MFCs equipped with different cathodes with tannery wastewater and operated them in open-circuit mode for 42 days to allow the electroactive biofilm to successfully acclimate to the alkaline environment (pH = 12.8). Fig. 4a shows a similar trend across all MFCs, with the potential output gradually increasing over time until it stabilizes at a maximum value within 250–300 h. Among all tested Tannery MFCs (TMF), Pt/C–TMFC exhibited the highest OCP (0.79 ± 0.12 V), which was comparable to PdO–MnO_2/rGO–TMFC (0.71 ± 0.03 V) and Ag_2O–MnO_2/rGO–NiPc–TMFC (0.67 ± 0.02 V), and much higher than that of the control TMFC (0.45 ± 0.01 V). Our results reveal that both the acclimation of anodic biofilm and cathodic materials govern the overall efficiency of MFC treating Cr(VI)-rich waste streams.

After the acclimatization process, we operated MFCs in a closed-circuit mode with an external resistance of 10 kΩ to improve electron transfer rates and generate net energy output. Potential output gradually increased, peaking within 100 h, then decreased as glucose was consumed by the electroactive biofilm. In addition, MFCs equipped with Pt/C outcompeted other tested TMFCs, with a maximum potential of 0.63 ± 0.05 V compared to only 0.39 ± 0.02 V, 0.45 ± 0.03 V, and 0.46 ± 0.007 V for the control MFC, PdO–MnO_2/rGO–TMFC, and Ag_2O–MnO_2/rGO–NiPc–TMFC (Fig. 4b). Similarly, Pt/C–TMFC and Ag_2O–MnO_2/rGO–NiPc–TMFC exhibited relatively higher power output at 24.76 mW m^{-3} (7.53 mW m^{-2}) and 21.14 mW m^{-3} (8.99 mW m^{-2}), respectively, compared to 19.94 mW m^{-3} (7.16 mW m^{-2}) for PdO–MnO_2/rGO–TMFC and 13.21 mW m^{-3} (4.64 mW m^{-2}) for the control TMFC (Fig. 4c). We estimated the internal resistances based on the polarization curves (Fig. 4d). Among all TMFCs, Pt/C–TMFC showed the lowest R_{in} (231 ± 1.6 Ω), surpassing all tested TMFCs (*i.e.*, 586 ± 1.2, 476 ± 4.8, and 445 ± 2.1 Ω for the control TMFC, PdO–MnO_2/rGO–TMFC, and Ag_2O–MnO_2/rGO–NiPc–TMFC) (Table 2). These results strongly suggest that microbial acclimatization and the cathode material play a significant role in enhancing power production by facilitating the biodegradation of complex tannery wastewater. Cr(VI) removal efficiency and CE in MFCs showed a similar trend to power generation, with Pt/C–MFC exhibiting the highest removal efficiency of 93.05 ± 2.35% and CE of 37.09± 4.85%, surpassing Ag_2O–MnO_2/rGO–NiPc–TMFC (90.14 ± 5.8% and 31.04± 3.08%), PdO–MnO_2/rGO–TMFC (85.83 ± 4.8% and 26.74 ± 3.16%), and control TMFC (73.61 ± 5.53% and

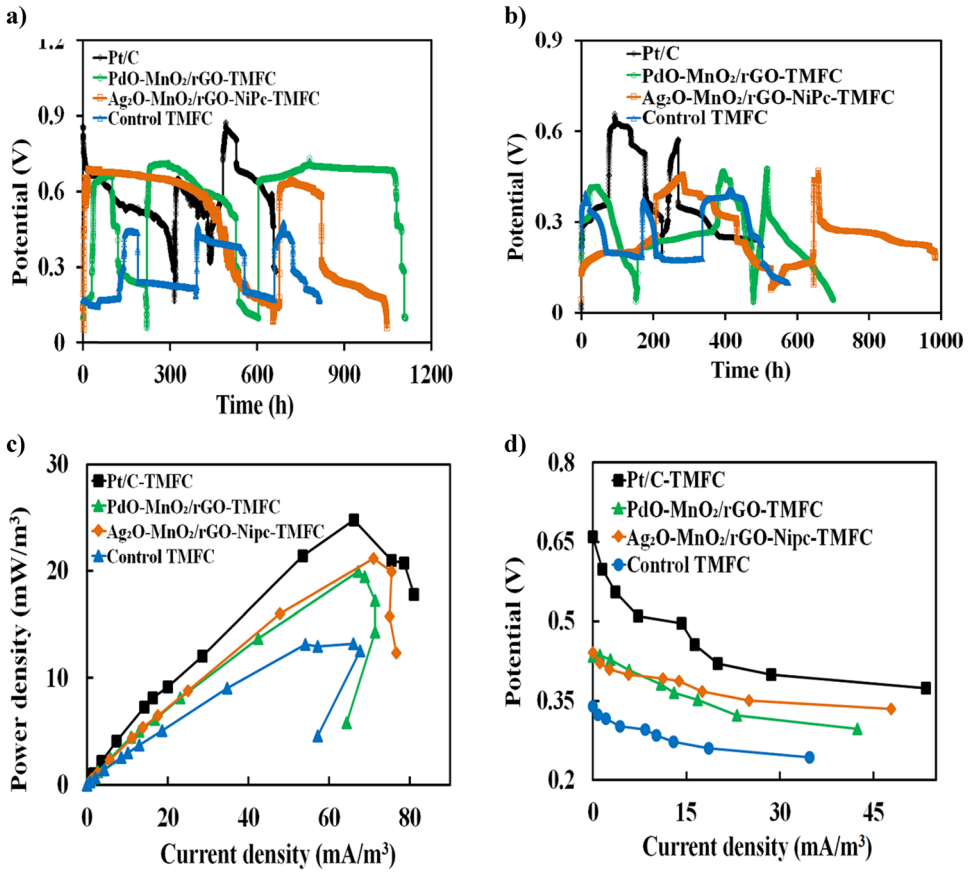

Fig. 4 Performance of MFCs fed with tannery wastewater (initial COD concentration = 7298 ± 616 mg L^{-1}): (a) open-circuit potential output, (b) closed-circuit potential output, (c) power curve, and (d) polarization curves.

21.1 ± 23.29%), respectively (Table 2). This study demonstrated that the biodegradation of tannery wastewater in MFCs involves both the anodic electrode and the selection of efficient cathodic electrocatalysts. Obviously, Pt/C performs better in real tannery wastewater because it was far more resistant to fouling and poisoning by the complex organic and inorganic constituents, and remains stable under extremely alkaline conditions compared to the other electrocatalysts.

3.4. Environmental implications

MFCs hold significant potential for renewable electricity generation from tannery wastewater, but their scale-up remains constrained by high material costs and limited substrate conversion efficiency, particularly when treating metal-rich waste streams. To address these limitations, scaling efforts must prioritize improving electron recovery and identifying cost-effective, durable cathode materials. Pt-based cathodes typically represent a major economic barrier to MFC deployment due to platinum's extremely high cost. Recent market analyses report Pt at approximately 62.22 USD per g, while common transition metals such as cobalt, manganese, nickel, and silver cost 10^3–10^4 times less, with cobalt priced at just 0.05279 USD per g. Commercial Pt/C catalysts were likewise expensive, with 10 wt% Pt/C sold at ~65 USD per g, corresponding to ~650 USD per gram of Pt actually loaded. Replacing Pt/C with Ag_2O–MnO_2/rGO–NiPc or PdO–MnO_2/rGO therefore reduces the raw catalyst material cost per electrode area by approximately one order of magnitude. Both PdO–MnO_2/rGO and Ag_2O–MnO_2/rGO–NiPc nanocomposites proved effective as cathode catalysts and electroactive surfaces for Cr(VI) reduction, with no detectable catalyst leaching during long-term operation. Another barrier was the deposition of Cr(III) solids (*e.g.*, $Cr(OH)_3$ and Cr_2O_3) on the biofilm and anodic electrodes during Cr(VI) reduction, which must be handled as hazardous or recoverable waste, and their safe removal or recovery is essential for long-term operation. Moreover, the highly alkaline conditions of

Table 2 Summary of electrochemical performance of MFCs fed with tannery wastewater

Parameter	Control TMFC	PdO–MnO_2/rGO–TMFC	Ag_2O–MnO_2/rGO–NiPc–TMFC	Pt/C–TMFC
R_{in} (Ω)	586 ± 1.2	476 ± 4.8	445 ± 2.1	231 ±1.6
Cr(VI) removal efficiency (%)	73.61 ± 5.53	85.83 ± 4.8	90.14 ± 5.8	93.05 ± 2.35
CE (%)	21.1 ± 23.29	26.74 ± 3.16	31.04 ± 3.08	37.09 ± 4.85

tannery wastewater (pH > 12) pose challenges for electrode stability, reactor materials, and microbial resilience, and scale-up would require engineering solutions such as pH conditioning, protective coatings, or alkaline-resistant materials.[54] It can be concluded that PdO–MnO_2/rGO and Ag_2O–MnO_2/rGO–NiPc nanocomposites have been instrumental as cathode catalysts while also serving as an electroactive surface for the reduction of Cr(VI). Consequently, this cost advantage, combined with their high ORR activity, chemical stability, and favorable long-term performance, highlights their promise as economically viable cathode materials for future MFC scale-up.

4. Conclusion

In this study, a robust electroactive anodic biofilm was developed under high chromate stress, with a minimum toxic concentration of 30 mg L^{-1}, demonstrating the consortium's ability to sustain substrate oxidation across a wide range of Cr(VI) concentrations. XPS analysis confirmed that Cr(VI) was primarily reduced to Cr(III) species, mainly $Cr(OH)_3$ and Cr_2O_3, through interactions with functional groups on the biofilm surface, highlighting the central role of the bioanode in both bioreduction and chromium speciation. The performance of the different cathode catalysts showed that the Ag_2O–MnO_2/rGO–NiPc and PdO–MnO_2/rGO nanocomposites enhanced power generation, Cr(VI) reduction, and coulombic efficiency in synthetic medium. While in real tannery wastewater, Pt/C–TMF and Ag_2O–MnO_2/rGO–NiPc–TMF demonstrated superior stability and electrochemical performance under complex, highly alkaline conditions. The integration of an acclimated bioanode with optimized cathode catalysts demonstrates the feasibility of single-chamber MFCs as a scalable, economically viable approach for combined Cr(VI) remediation and energy recovery in industrial wastewater treatment.

Author contributions

Dena Z. Khater: conceptualization, investigation, methodology, formal analysis, data curation, visualization, validation, and writing – original draft. Rabab S. Amin: conceptualization, investigation, methodology, formal analysis, data curation, visualization, validation, and writing – review and editing. Amani E. Fetohi: conceptualization, investigation, methodology, formal analysis, data curation, visualization, validation, and writing – review and editing. Mohamed Mahmoud: conceptualization, investigation, methodology, formal analysis, data curation, visualization, validation, resources, and writing – review and editing. Kamel M. El-Khatib: conceptualization, investigation, methodology, formal analysis, data curation, visualization, validation, funding acquisition, writing – review and editing, and supervision.

Conflicts of interest

The authors declare that they have no known competing financial interests or personal relationships that could have influenced the work reported in this paper.

Data availability

The datasets used and/or analyzed during the current study are included in the article.

Acknowledgements

This work was carried out in the framework of the India–Egypt bilateral project agreement on science and technology cooperation (Grant number: 4429). The authors would like to thank the Academy of Scientific Research and Technology (ASRT), Egypt, for its support. Furthermore, the authors would like to thank the National Research Centre for providing all the research facilities for this work.

References

1 N. Timothy and E. T. Williams, *Int. J. Environ. Chem.*, 2019, **3**, 72–82.
2 M. M. Ali, D. Hossain, M. S. Khan, M. Begum and M. H. Osman, *Heavy metals-their environmental impacts and mitigation*, IntechOpen, 2021.
3 M. Tumolo, V. Ancona, D. De Paola, D. Losacco, C. Campanale, C. Massarelli and V. F. Uricchio, *Int. J. Environ. Res. Public Health*, 2020, **17**, 5438.
4 A. R. P. Hidayat, L. L. Zulfa, D. Prasetyoko, R. Abdullah, E. N. Kusumawati, H. Bahruji, B. T. I. Ali, R. A. Salsabila and R. Ediati, *J. Water Process Eng.*, 2025, **69**, 106843.
5 A. Baral and R. D. Engelken, *Environ. Sci. Policy*, 2002, **5**, 121–133.
6 S. S. Kerur, S. Bandekar, M. S. Hanagadakar, S. S. Nandi, G. M. Ratnamala and P. G. Hegde, *Mater. Today Proc.*, 2021, **42**, 1112–1121.
7 H. Assefa, S. Singh, F. E. Olu, D. S. Dhanjal, D. Mani, N. A. Khan, J. Singh and P. C. Ramamurthy, *Desalination Water Treat.*, 2024, **319**, 100576.
8 S. Hossan, S. Hossain, M. R. Islam, M. H. Kabir, S. Ali, M. S. Islam, K. M. Imran, M. Moniruzzaman, T. J. Mou and A. K. Parvez, *Int. J. Environ. Res. Public Health*, 2020, **17**, 6013.
9 P. Seragadam, A. Rai, K. C. Ghanta, B. Srinivas, S. K. Lahiri and S. Dutta, *Biodegradation*, 2021, **32**, 449–466.
10 R. Jobby, P. Jha, A. K. Yadav and N. Desai, *Chemosphere*, 2018, **207**, 255–266.
11 R. Esmat, A. Ghorab, A. Pugazhendi, M. T. Jamal, R. Banu, J. Jacques and D. Kumar, *Environ. Res.*, 2022, **212**, 113304.
12 C. Fang and V. Achal, *Microorganisms*, 2019, **7**, 697.
13 S. Z. Abbas, M. Rafatullah, N. Ismail and M. I. Syakir, *Int. J. Energy Res.*, 2017, **41**, 1242–1264.

14 R. Rafieenia, M. Mahmoud, F. El-Gohary and C. A. Rossa, *Sustainable Energy Technol. Assess.*, 2022, **54**, 102805.
15 R. Rafieenia, M. Sulonen, M. Mahmoud, F. El-Gohary and C. A. Rossa, *Sci. Total Environ.*, 2022, 153923.
16 L. Shi, H. Dong, G. Reguera, H. Beyenal, A. Lu, J. Liu, H.-Q. Yu and J. K. Fredrickson, *Nat. Rev. Microbiol.*, 2016, **14**, 651–662.
17 M. El-Qelish and M. Mahmoud, *Sci. Total Environ.*, 2022, **802**, 149851.
18 M. Mahmoud and K. M. El-Khatib, *Int. J. Hydrogen Energy*, 2020, **45**, 32413–32422.
19 M. Mahmoud, C. I. Torres and B. E. Rittmann, *Environ. Sci. Technol.*, 2017, **51**, 13461–13470.
20 C.-W. Lin, Y.-C. Jhan, T.-J. Zhu and S.-H. Liu, *J. Water Process Eng.*, 2023, **53**, 103612.
21 Z. An, H. Zhang, Q. Wen, Z. Chen and M. Du, *Desalination*, 2014, **354**, 181–188.
22 D. Z. Khater, R. S. Amin, A. E. Fetohi, M. Mahmoud and K. M. El-Khatib, *Sci. Rep.*, 2023, **13**, 20184.
23 Z. Li, X. Zhang and L. Lei, *Process Biochem.*, 2008, **43**, 1352–1358.
24 C. Wang, H. Deng and F. Zhao, *Soil Sediment Contam.*, 2016, **25**, 1–12.
25 D. Z. Khater, R. S. Amin, A. E. Fetohi, K. M. El-Khatib and M. Mahmoud, *Sustainable Energy Fuels*, 2022, **6**, 430–439.
26 M. Mahmoud, T. A. Gad-Allah, K. M. El-Khatib and F. El-Gohary, *Bioresour. Technol.*, 2011, **102**, 10459–10464.
27 D. Khater, R. S. Amin, M. O. Zhran, Z. K. Abd El-Aziz, M. Mahmoud, H. M. Hassan and K. M. El-Khatib, *J. Genet. Eng. Biotechnol.*, 2022, **20**, 12.
28 R. Kumar, M. Mooste, I. Zekker, M. Käärik, J. Leis, A. Kikas, A. Treshchalov, J. Kozlova, M. Otsus and J. Aruväli, *Int. J. Hydrogen Energy*, 2025, **98**, 793–806.
29 M. J. Uddin, Y.-K. Jeong and W. Lee, *Int. J. Hydrogen Energy*, 2021, **46**, 11458–11481.
30 C. Orak, *RSC Adv.*, 2024, **14**, 34356–34361.
31 K. Fei, T. Song, H. Wang, D. Zhang, R. Tao and J. Xie, *R. Soc. Open Sci.*, 2017, **4**, 170798.
32 J. Ali, L. Wang, H. Waseem, R. Djellabi, N. A. Oladoja and G. Pan, *Chem. Eng. J.*, 2020, **384**, 123335.
33 D. Z. Khater, R. S. Amin, A. E. Fetohi, M. Mahmoud and K. M. El-Khatib, *J. Power Sources*, 2024, **591**, 233809.
34 D. Z. Khater, R. S. Amin, A. E. Fetohi, M. M. Mahmoud and K. M. El-Khatib, *J. Environ. Chem. Eng.*, 2025, **13**(4), 117304.
35 APHA/AWWA/WEF, American Public Health Association, 2017, 8.
36 M. Mahmoud, P. Parameswaran, C. I. Torres and B. E. Rittmann, *Bioresour. Technol.*, 2014, **151**, 151–158.
37 P. Zhang, C. Yang, Y. Xu, H. Li, W. Shi, X. Xie, M. Lu, L. Huang and W. Huang, *Bioresour. Technol. Rep.*, 2019, **8**, 100347.
38 M. Mahmoud, P. Parameswaran, C. I. Torres and B. E. Rittmann, *Biotechnol. Bioeng.*, 2017, **114**, 1151–1159.
39 R. Esmat, A. Ghorab, A. Pugazhendi, M. T. Jamal, R. Banu, J. Jacques and D. Kumar, *Environ. Res.*, 2022, **212**, 113304.
40 Z. Rahman and L. Thomas, *Front. Microbiol.*, 2021, **11**, 1–19.
41 Q. Wang, C. Zhang, J. Song, B. Bamanu and Y. Zhao, *J. Hazard. Mater.*, 2024, **472**, 134447.
42 X. Luo, X. Zhou, C. Peng, P. Shao, F. Wei, S. Li, T. Liu, L. Yang, L. Ding and X. Luo, *J. Hazard. Mater.*, 2022, **433**, 128822.
43 A. Arishi and I. Mashhour, *J. Pure Appl. Microbiol.*, 2021, **15**, 53–67.
44 Q. Zeng, Y. Hu, Y. Yang, L. Hu, H. Zhong and Z. He, *J. Hazard. Mater.*, 2019, **368**, 149–155.
45 C. Yang, Y. Xin, C. Huiying, K. Yaru, L. Mengmeng and Y. Sailong, *Appl. Phys. A*, 2021, **127**, 1–9.
46 Y. Luo, Y. Wu, D. Wu, C. Huang, D. Xiao, H. Chen, S. Zheng and P. K. Chu, *ACS Appl. Mater. Interfaces*, 2020, **12**, 42850–42858.
47 Q. An, S. Deng, J. Xu, H. Nan, Z. Li and J. Song, *Ecotoxicol. Environ. Saf.*, 2020, **191**, 110001.
48 Z.-H. Mengke-Li, Y. Z. Yuting-Zhuo, Y. H. Yuting-Hu, S. L. Shuzhen-Li, L. H. Liang-Hu and H. Z. Hui-Zhong, *Ecotoxicol. Environ. Saf.*, 2019, **184**, 109636.
49 H. Wang and Z. J. Ren, *Water Res.*, 2014, **66**, 219–232.
50 P. Ganesan, A. Ishihara, A. Staykov and N. Nakashima, *Bull. Chem. Soc. Jpn.*, 2023, **96**, 429–443.
51 H. Hao, X. Zhou, J. Liang and W. Shen, *J. Mater. Chem. C*, 2026, **14**, 2174–2207.
52 F. Lachquer, N. Touach, A. Benzaouak and J. Toyir, *Processes*, 2026, **14**, 440.
53 C. Saran, D. Purchase, G. D. Saratale, R. G. Saratale, L. F. R. Ferreira, M. Bilal, H. M. N. Iqbal, C. M. Hussain, S. I. Mulla and R. N. Bharagava, *Chemosphere*, 2023, **312**, 137072.
54 S. G. Peera, T. Maiyalagan, C. Liu, S. Ashmath, T. G. Lee, Z. Jiang and S. Mao, *Int. J. Hydrogen Energy*, 2021, **46**, 3056–3089.